Modeling of Prebreakdown VI Characteristics of a Wire-plate Electrostatic Precipitator Operating under Combined dc-pulse Energization

B. S. Rajanikanth and B. R. Prabhakar

Department of HV Engineering,
Indian Institute of Science, Bangalore, India

ABSTRACT

With the advent of pulse energization in electrostatic precipitators, the need for developing a model to simulate the physical processes in the prebreakdown region, at which the precipitator normally operates, is also increasing. The development of such a model helps in predicting the VI characteristics of a precipitator, which will be important to diagnose the electrical problems associated with the precipitator during its operation. The paper reports the details of a proposed model to predict the VI characteristics of a wire-plate precipitator operating under the influence of repetitive pulses superposed on a dc bias. The model begins with the calculation of space charge density near the HV electrode during the pulse-on period and then proceeds with the drift of space charges in the pulse-off period aided by the dc bias. The pulse duration was $\sim$ 250 ns. The pulse repetition rate was 50 Hz. The predicted results were validated against the experimental results conducted on a laboratory model of a wire-plate precipitator. The studies were conducted for dust free conditions.

1. INTRODUCTION

IN an electrostatic precipitator (ESP) the voltage-current (VI) characteristics are important in diagnosing the electrical problems associated with it during its operation. The VI characteristics are easy to measure and provide most of the information required. The VI characteristics in dust free or clean air conditions are considered as the reference and it should be measured under ambient load before the ESP is put into operation, soon after startup, and twice a month thereafter.

The mathematical modeling of VI characteristics of an ESP makes feasible analysis of current and voltage for various wire sizes, plate-plate spacings and wire-wire spacings when the device is in the design stage. The model can be used also to analyze the effects of different operating conditions on the ESP performance.

It is essential to make several assumptions in developing a mathematical model. It is assumed that the electrodes are clean, that the discharge electrodes are smooth round wires and the corona discharge is distributed uniformly over the surface of the wires. These simplifying assumptions, however, have been of considerable value in developing the science of precipitation and the resultant equations give good insight into the behavior of the electric field and current density. Also, the equations can be used to calculate average values of the field and current density which are suitable for some aspects of precipitator modeling.

The electrical conditions inside a precipitator are mainly governed by the applied electric field and the corona generated space charge density distributions. The solution to the differential equations relating the electric field and the charge density in a duct type ESP are difficult to

1070–9878/94/$3.00

obtain because the differential equations cannot be solved analytically as is the case with pipe type or wire-cylinder ESP, the electric field and the space charge density due to ions are strongly related to each other and both are functions of position, and finally the ions have different mobilities which are functions of position and field.

Study of the literature on the theoretical aspects of precipitation indicates that much work has been done on the mathematical modeling of VI characteristics of ESP operating under dc energization. Only recently much interest is being shown in the development of a similar model for a pulse operated ESP.

Sekar and Stomberg [1] have developed a theoretical model for prediction of space charge and field conditions for pulsed corona in a wire-cylinder type ESP. The pulse width investigated was in the range of 100 to 300 μs. They have observed that as the pulse width is changed the charge per pulse does not vary proportionally, but depends on the pulse magnitude.

Menegozzi and Feldman [2] developed a quasi steady state model to predict the charge density near the discharge electrode of a wire-cylinder type ESP operating under pulse energization, with pulse widths in the range of 2 to 5 μs. Salasoo *et al.* [3] developed a model to simulate the corona process, in both space and time, for a wire-cylinder type ESP. The model permits estimation of ion densities and field distribution for various pulse parameters. They have validated the model with the test results conducted under clean air conditions.

It is seen from the literature [4] that the application of microsecond rise time pulse technology to ESP has already reached full industrial demonstration, and that reliable equipment is available. The literature also indicates the importance of nanosecond or sub-microsecond pulse energization in ESP, particularly in preventing back corona as well as in the simultaneous removal of gaseous pollutants along with the solid particulate from flue gases. Only recently work has been initiated to simulate the corona process in a sub-microsecond pulse energized ESP with the aim of predicting its VI characteristics.

The earlier mathematical models have been developed for wire cylinder type ESP though it is the wire-plate type (duct type) ESP which is widely used. This paper reports the development of a 2-dimensional space-time model simulating the clean air VI characteristics of a duct type ESP. As a first attempt, only pulses of nanosecond rise time were considered. The predicted results were validated against the carefully conducted experimental results.

2. MATHEMATICAL MODELING OF PULSE VI CHARACTERISTICS

The VI characteristics provide important design data on the electrical performance of the wire-plate geometry of the ESP. However, to achieve optimum conditions of operating voltage, wire-wire spacing and duct spacing, considerable experimental work on actual ESP system is involved which is very expensive and time consuming. Hence, it would be of great help if the system is represented as a mathematical model, based on the actual physical processes taking place in the ESP. The work described in this section is aimed at modeling the pulse VI characteristics of a duct type ESP.

It is well known that negative corona is used in the precipitation process because of its higher sparkover voltage and superior VI characteristics [5]. Negative corona discharges, either dc or pulse energized, occur in the form of very short pulses with a voltage dependent repetition rate [6, 7]. These pulses were studied in detail first by Trichel [8] and these pulses are now called as Trichel pulses.

It has been shown that while a 1-dimensional model is adequate to describe the ionization phase of a Trichel pulse, the same is insufficient for modeling the drift of space charges and one has to use a 2-dimensional model for good results. For adequate study of ESP performance under pulse energization, the behavior of the ionization zone near the discharge electrode must be addressed apart from the simulation of drift of charges in the interelectrode space.

The proposed model has been developed in two parts. The first part calculates the ion space charge density near the wire during the pulse-on period and the second part calculates the drift of the space charge from the wire towards the collectors, during the pulse-off period. The drift, during the pulse-off period, is mainly governed by the applied dc bias. At the end of the pulse-off period the current density near the collector is compared with the specified boundary value and if necessary, the entire process is repeated by incrementing the pulse voltage and calculating a new space charge density near the wire for this new pulse voltage. For the second part of the model the solution is obtained by solving the Poisson equation and the time dependent current continuity equation using a 2-dimensional approach and subjected to certain boundary conditions specified in [9].

2.1. CALCULATION OF SPACE CHARGE DENSITY NEAR THE WIRE

2.1.1. DEVELOPMENT OF THE MODEL

It has been shown in [9] that the corona activity near the wire is almost the same for a wire-plate and an equiv-

alent wire-cylinder geometry *i.e.* the radius of the region immediately near the wire where ionization occurs is approximately the same for both cases. This is reasonable since the characteristics of the region of ionization will depend primarily on the electric field near the wire. Evidence in support of this assumption can be found in the fact that the corona onset voltage for a wire-cylinder geometry is only 6% less than that of a duct type ESP having a wire-plate spacing equivalent to that of a wire-cylinder type [10]. With this simplification, the 2-dimensional wire-plate geometry reduces to 1-dimensional wire-cylinder geometry. But this approximation is restricted only to the calculation of space charge density near the wire.

Now, it is of interest to determine the number of Trichel pulses present in the applied voltage pulse which is having a width of 700 ns and a rise time of 250 ns. Based on the arguments made in [2], the estimates of the times involved in different stages of the Trichel pulse discharge are $t_r = 250$ ns rise time of the voltage pulse, $t_d = 700$ ns pulse width, $t_a \simeq 30$ to 50 ns avalanche transit time [11], $t_c \simeq 10t_a \simeq 300$ to 500 ns space charge buildup time, [2, 12] V_e = electron drift velocity, and $\vec{E}$ = applied electric field.

Aleksandrov [12] has shown that the Trichel pulse develops in two stages. The first stage is a long lasting stage of 300–500 ns and the second is $\sim$ 10 to 15 ns [6, 13]. The time elapsed during the two stage development of the Trichel pulse and final quenching is comparable to the pulse voltage parameters used in the present work *i.e.* $t_c \simeq t_d$. Also, voltage pulses of duration within the microsecond range, do not contribute much to the sweeping of ions away from the cathode. This sweeping is essentially done by the dc bias voltage in conjunction with the space charge field. Thus the pulse is mainly a charge producing field. Since the ions created by pulse move away very little from the wire during the pulse-on period, the quenching of the discharge should last for a time considerably longer than the pulse width t_d. In other words, every voltage pulse would be able to create only a single Trichel or space charge pulse. So, it is sufficient to model only one Trichel pulse during the pulse regime in the present case.

The basic equations coupling the field and charged particles can be written, neglecting ion diffusion and recombination effects, as

$$\nabla \cdot \vec{E} = \frac{\rho_p \rho_n}{\epsilon_o} \tag{1}$$

$$\nabla \cdot \vec{J_e} + \frac{\partial \rho_e}{\partial t} = (\alpha - \eta)\rho_e V_e \tag{2}$$

$$\nabla \cdot \vec{J_n} + \frac{\partial \rho_n}{\partial t} = \eta \rho_e V_e \tag{3}$$

$$\nabla \cdot \vec{J_p} + \frac{\partial \rho_p}{\partial t} = \alpha \rho_e V_e \tag{4}$$

Equation (1) is the well known Poisson's equation. Equations (2) to (4) are the current continuity equations for electrons, negative ions and positive ions respectively. ρ is the space charge density and subscripts e, n and p stand respectively for electrons, negative ions and positive ions. α and η stand respectively for Townsend's first ionization and attachment coefficients.

Since, in the present case, a wire-cylinder geometry is being considered for the calculation of space charge density and by making use of the discussion in the previous Section, simplifications can be made on the above set of equations. In [2] it has been shown that, given the pulse characteristics, where $t_r \simeq 200$ to 300 ns and $t_d \simeq 2$ to 4 μs, the main features of the corona discharge will not be affected if the steep rise pulses are substituted by square wave pulses having a width t_d and amplitude given by the average value of the pulse voltage. Now $V_p(t)$, the pulse voltage, can be approximated as [2]:

$$V_p(t) \simeq V_m \frac{t}{t_m} \exp\left[1 - (t/t_m)\right] \tag{5}$$

where at $t = t_m$, $V_p(t) = V_m$ = peak value of the voltage. Now, the average value of $V_p(t)$ is given by

$$\begin{aligned} \langle V_p \rangle &= \frac{1}{t_d} \int_0^{t_d} V_p(t)\, dt \\ &= V_m \frac{t_m}{t_d} \left[e^1 - e^{1-[t_d/t_m]} \left(1 + [t_d/t_m]\right) \right] \end{aligned} \tag{6}$$

Since in the present case the values of t_r and t_d, fall well within the range studied by Feldman and Menegozzi, the above assumption holds. Also, the ionization and attachment times are much less than the avalanche formation and space charge buildup times, one can reasonably assume that during the presence of steep fronted pulses, the Townsend avalanches will develop as if they were produced by an equivalent dc voltage of magnitude $V \simeq V_d + \langle V_p \rangle$. After the pulse regime, the field will be governed solely by V_d and that due to ionic space charges. The above approximation is valid only if $t_d \simeq t_c$. The details of the solution to the Equations (1) to (4) are given in [2]. Only the final simplified form of the equations are presented here. They are:

$$E(r) = \frac{1}{r} \left(r_o\, E(r_o, t) \; - \frac{q}{2\,\pi\,\epsilon_o} \left[N_p(r) - N_n(r) \right] \right) \tag{7}$$

$$N_e(r) = N_o \exp\{ \int_{r_o}^{r} \alpha(r') - \eta(r') \}\, dr' \tag{8}$$

$$N_p(r) = N_o \int_{r_o}^{r} \alpha(r') \exp\left[\int_{r_o}^{r'} \big(\alpha(r'') - \eta(r'')\big) dr''\right] dr' \tag{9}$$

$$N_n(r) = N_o \int_{r_o}^{r} \eta(r') \exp\left[\int_{r_o}^{r''} \big(\alpha(r'') - \eta(r'')\big) dr''\right] dr' \tag{10}$$

where r_o = Radius of the corona wire, q = electron charge, N_o = initial number of electrons at the cathode, N_e, N_p, and N_n are respectively the cumulative number of electrons, positive ions and negative ions, per unit length of the wire.

The filed at the cathode should be found out using the boundary condition

$$\int_{r_o}^{R} E(r,t) = V_d + V_p(t) \tag{11}$$

where R = wire to cylinder spacing, V_d = dc voltage, and $V_p(t)$ = pulse voltage.

The continuity equations for positive and negative ions are solved with the boundary condition setting N_p at anode and N_n at cathode, to zero. For the continuity equation for electron, the boundary condition is that the electron density at the cathode N_o should be equal to

$$N_o = N_{ph} + N_i \tag{12}$$

where N_{ph} = number of secondary electrons released by gas produced photons (photoemission), and N_i = number of secondary electrons produced by positive ion impact.

In the present case, since the duration of voltage pulses is very short, the photoemission is considered to be the only possible secondary mechanism for the generation of secondary electrons. The number of photoelectrons produced at the cathode [14] is given by

$$N_{ph} = N_o \Gamma_p \int_{r_o}^{r_i} \alpha(r)\, g(r)\, \exp[-\mu' r] \times \left[\exp\{\int_{r_o}^{r} \alpha(r') - \eta(r')\} dr'\right] dr \tag{13}$$

where Γ_p = coefficient of secondary ionization by photoemission, μ' = absorption coefficient for photons in the gas, r_i = radius of ionization layer at which $\alpha = \eta$, and $g(r)$ = geometrical factor representing the proportion of photons that may reach the cathode.

The geometric factor $g(r)$ is given approximately [15] in terms of its radial and axial components as:

$$g(r) = g_{axi}(r) \times g_{rad}(r) \tag{14}$$

where

$$g_{rad}(r) = A_o \int_{0}^{\sin \frac{r}{r_o}} \exp(-\mu' \sqrt{r^2 + r_o^2 - 2 r r_o \cos\phi})\, d\phi \tag{15}$$

$$g_{axi}(r) = A_o \int_{0}^{\frac{\pi}{2}} \exp(-\mu' [r - r_o] / \cos\phi)\, d\phi \tag{16}$$

where $A_o = 1/\{\pi \exp[-\mu'(r - r_o]\}$ The condition for self sustained discharge is $N_{ph} > 1$. It is to be noted that the ionization region extends from the cathode to the boundary at which ionization and attachments coefficients are equal. The attachment region starts at this point and extends to the region at which 99% of the electrons get attached to neutral molecules forming negative ions [16]. That is, attachment region extends from the point at which $\alpha = \eta$ to the point at which $\alpha \ll 0.1$.

2.1.2. DATA FOR NUMERICAL CALCULATIONS

The numerical calculations are performed for negative corona discharge in air at atmospheric pressure. The data for the calculations are taken from various literature. The ionization and attachment coefficients can well be represented by the equations of the type:

$$\alpha/p = A \exp[-B\,(p/E)] \tag{17}$$

$$\eta/p = C + D\,(E/p)^2 + F\,(E/p) \tag{18}$$

where p = atmospheric pressure in Pa E = electric field in V/cm.

The constants A, B, C, D and F are determined by curve fitting the experimental results on ionization and attachment data [15]. Accordingly For $0.19 < E/p < 0.45$, the values are $A = 4.778$; $B = 221$; $C = 0.01298$; $D = -541\times10^{-6}$; $F = 0.87\times10^{-5}$, and for $0.45 < E/p < 1.82$, the values are $A = 9.68$ and $B = 264$.

But for $E/p < 0.19$ and $E/p > 0.45$, the value of the attachment coefficient is not known. Ogasawara [17] has used a different equation to fit the experimental data of attachment valid over a wide range of E/p (0.08 to 3.8). It is of the form

$$\eta/p = \frac{C\,(E/p)^2 - D\,(E/p) + F}{(E/p)^8 + G} \tag{19}$$

where $C = 4.199\times10^{10}$, $D = 2.623\times10^{12}$, $F = 6.15\times10^{13}$ and $G = 4.473\times10^{15}$.

Equation (19) has been used in the present calculations. In Equation (13) the secondary ionization coefficient Γ_p due to photons, is taken to be 5×10^{-5} [12, 15], for negative corona in air. The absorption coefficient $\mu \approx 6$ cm^{-1} for air is [14]. The initial number of electrons which

start the first avalanche is taken as 1 [11]. The starting field for the primary avalanche is given by

$$E(r) = \frac{V_d + \langle V_p \rangle}{r \log(R/r_o)} \tag{20}$$

2.1.3. METHOD OF SOLUTION

The Equations (5) to (19) describe the process of negative corona discharge in a wire-cylinder geometry for time scales less than t_c. The calculations begin under the influence of the Laplacian field governed by Equation (20). The electronic and ionic charge densities are computed using Equations (8) to (10). The integration is carried out in steps with a step size equal to $1/\alpha(r)$ in the ionization region and $1/\eta(r)$ in the attachment region; *i.e.* for any two grid points j and $j+1$, we have $r_{j+1} = r_j + 1/\alpha(j)$ in the ionization region and $r_{j+1} = r_j + 1/\eta(j)$ in the attachment region.

The selection of this step size is reasonable since the step sizes are the ionization free and attachment free path lengths in the respective regions, as the avalanche proceeds from the cathode to the low field regions. Ionization stops once $\alpha = \eta$ and electron density decreases from there on as more and more electrons get attached to form negative ions and at the end of the attachment region almost all electrons would have converted to negative ions. After this region the step size for the integration can be increased suitably.

Once the space charge density is computed, the distorted field is calculated using Equation (7). The number of secondary electrons generated by photons produced within the ionization region, is calculated from Equation (13). The second generation avalanche takes place with this new secondary electrons as the starting electrons and the avalanche progresses under the distorted field conditions and thereby accumulation of positive and negative ions increases. Large field distortions due to the accumulated space charge lead to gradual narrowing of the ionization region and electron attachments start occurring closer and closer to the cathode [7]. This is being reflected in the decrease in number of photoelectrons in the second generation. Thus the contribution of successive avalanche generations *i.e.* the field $E(r)$, space charge density and the number of photoelectrons were monitored in each iteration and the discharge will be finally quenched once the number of photoelectrons goes below 1. The total number of the negative ions at the end of the discharge is then calculated. Since $1/\eta$ represents the average distance traveled by an electron before attachment, the size of the negative ion cloud at the end of the attachment region is given by

$$r_{neg} = r_1 + 1/\eta_{r_1} \tag{21}$$

where r_{neg} = outer boundary of negative ion cloud, r_1 = radius at which $\alpha = 0.1$, and $\eta_{r_1} = \eta$ at r_1.

Then if N_n is the total number of negative ions per unit length of wire before quenching, the average negative ion density N_{ave}, is given by

$$N_{ave} = \frac{N_n}{\pi\,(r_{neg}^2 - r_o^2)} \tag{22}$$

With this calculation of negative ion density the first part of the pulse model is completed.

2.2. DRIFT OF THE IONIC SPACE CHARGE AND PREDICTION OF *VI* CHARACTERISTICS

In this second part of the model the 2-dimensional model of the wire-plate geometry is taken into account. The negative space charge density near the wire, as calculated from the first part of the model, is taken as the known variable. Now, the drift of this space charge towards collector has to take place under the influence of dc bias only, which is kept at or below corona onset, for a period determined by the pulse repetition rate.

Neglecting the variation of voltage or current in the direction of the corona wire and neglecting the attachment of electrons after the attachement region, the Poisson's equation and the current continuity equations that are applicable to this part of the model are

$$\frac{\Delta^2 V}{\Delta x^2} + \frac{\Delta^2 V}{\Delta y^2} = \frac{\rho}{\epsilon_o} \tag{23}$$

$$\mu \left[\frac{\partial(\rho_x\, E_x)}{\partial x} + \frac{\partial(\rho_y\, E_y)}{\partial y} \right] = \frac{-\partial \rho_n}{\partial t} \tag{24}$$

A constant average mobility (μ) for the negative ions has been considered in Equation (24).

Applying backward difference approximation for the *space* and forward difference approximation to the *time* [18], we get

$$-\frac{\rho^{t+1} - \rho^t}{\Delta t} = \mu \left[\frac{\rho_x E_x - \rho_{x-1} E_{x-1}}{\Delta x} + \frac{\rho_y E_y - \rho_{y-1} E_{y-1}}{\Delta y} \right] \tag{25}$$

$$\rho_{i,j}^{t+1} = \rho_{i,j}^t - \frac{\mu\,\Delta t}{\Delta x} [\rho_{i,j}\, E_{i,j} - \rho_{i-1,j}\, E_{i-1,j}] - \frac{\mu\,\Delta t}{\Delta y} [\rho_{i,j}\, E_{i,j} - \rho_{i,j-1}\, E_{i,j-1}] \tag{26}$$

The time step taken for the computations must be limited by the Courant-Friedricks-Lewy condition [13] *i.e.*

$$\Delta t \ll \frac{\Delta x}{\mu\, E_x}\ ,\ \Delta t \ll \frac{\Delta y}{\mu\, E_y} \tag{27}$$

2.3. METHOD OF SOLUTION

The assumptions made in solving the Equations (23) and (26) are [1]:

1. Thickness of the corona ionization or corona zone is negligible.
2. The region outside the corona zone, called space charge zone, is assumed to contain unipolar ions.
3. Thermal diffusion of ions is neglected.
4. Variation of voltage or current density in the direction of the corona electrode (wire) is neglected, reducing the model to a 2-dimensional one.
5. Mobilities of the ions are described by a single effective mobility.

Figure 1(a) shows the solution domain in the wire-plate precipitator. Symmetry conditions reduce the area over which the equations must be evaluated, to a rectangle between the midline of the precipitator and one collector plate and extending along the midline axis from one corona wire to a point halfway between corona wires. Hence, it is necessary to solve the equations only over the rectangle ABCD as shown in the Figure. It is assumed that the solution will hold for similar rectangles within the precipitator. In this manner the entire two dimensional area can be taken into account.

The finite difference method was used to solve the system equations. The entire area of interest is divided into fine rectangular grids. Figure 1(b) shows a partial grid. 'O' refers to the computational point of interest. Once E and ρ are calculated here, the label O is moved to the neighboring point and the calculation repeated. Applying center difference approximations to Poisson's equations, the potential V at any point O can be written as

$$V_o = \frac{a_y^2(V_2 + V_4) + a_x^2(V_1 + V_3) + a_x^2 a_y^2 \frac{\rho_o}{\varepsilon_o}}{2(a_x^2 + a_y^2)} \qquad (28)$$

The following boundary conditions are applicable to the specified domain ABCD. $E_x = 0$ along line AB, $E_y = 0$ along lines BC, CD and AD, $V = 0$ on the collector electrode or along line CD, $V = V_o$ along the wire surface, $E_x = E_y = 0$ at points A and B, $\rho = \rho_c$, the space charge density at the wire and hence $\rho = \rho_c$ at point A, and $\rho = \frac{J_p}{\mu E_x}$ on the collector electrodes, where J_p is the average current density on the collector plate.

The field at the cathode is not at corona onset but at the value given by [19] as

$$E(r_o) = \frac{V_d}{r_o \log(4R/\pi r_o)} \qquad (29)$$

The above equation is valid for dc voltages below corona onset.

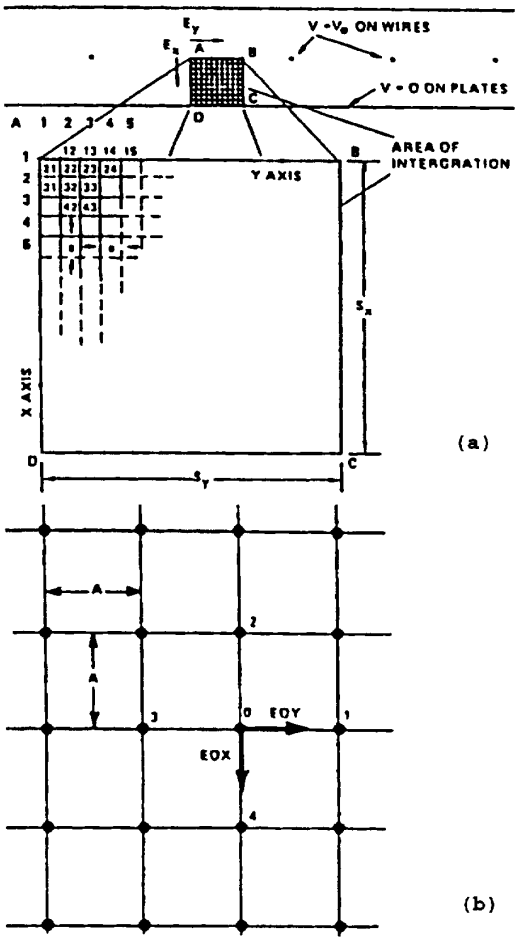

Figure 1.

Numerical solution domain of the wire-plate ESP [9]. (a) Nomenclature used for the solution domain, S_y = one half wire to wire spacing; S_x = wire to plate spacing; a = step size for integration; V_o = applied voltage; E_x = field component perpendicular to the plate; E_y = longitudinal component; J = average current density; (b) Partial grid of the solution domain.

Once the charge density is found from Equation (22), the distribution of the density at $t = 0$ (the time scale has been shifted so that $t = 0$ corresponds to $t = t_d$) is determined initially by making use of the quadratic relation derived for space charge density [9]. The field at the wire is given by Equation (29). An initial distribution of potentials is found out using Cooperman's equation [1]. Once the potential grid is formed, a new space charge density grid at $t = t_o + \Delta t$, where t_o is the time elapsed, is formed using Equation (26). With this new space charge values the change in the potential distribu-

tion is evaluated again by solving the Poisson equation by successive over-relaxation technique. This procedure is repeated until the time t = period between the pulses, T. In the present case T≈ 20 ms. At the end of T, if the computed average current density at the plate equals the chosen boundary value, then the computation stops. If not, the pulse voltage is incremented and the whole procedure is repeated starting from the first part of the model, to calculate a new negative ion density near the wire.

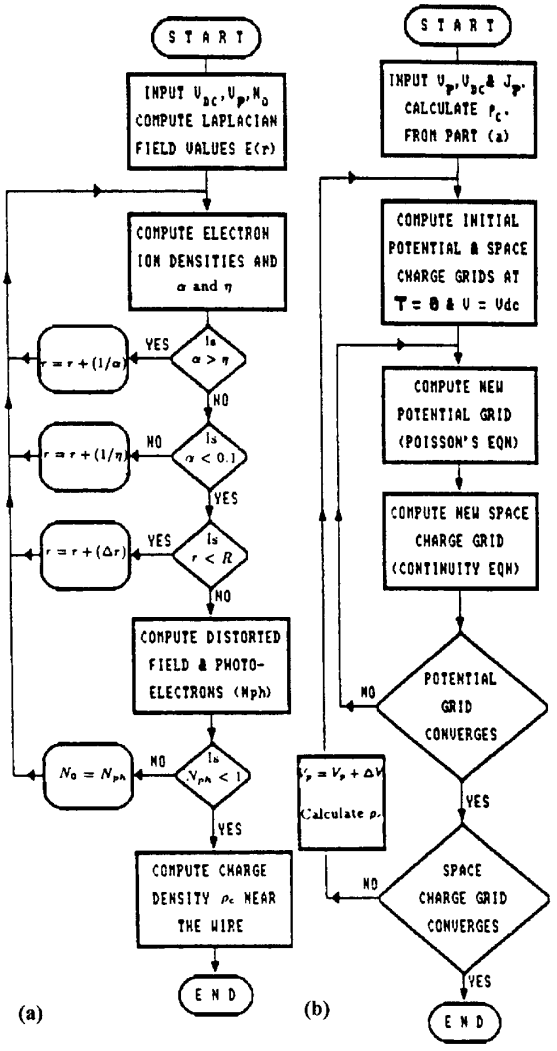

Figure 2.

Flow chart of the dc + pulse model. (a) First part of the pulse model, (b) second part of the pulse model.

Figure 2 shows the complete flow chart of the pulse model. The grid size chosen was 15×15. The convergence

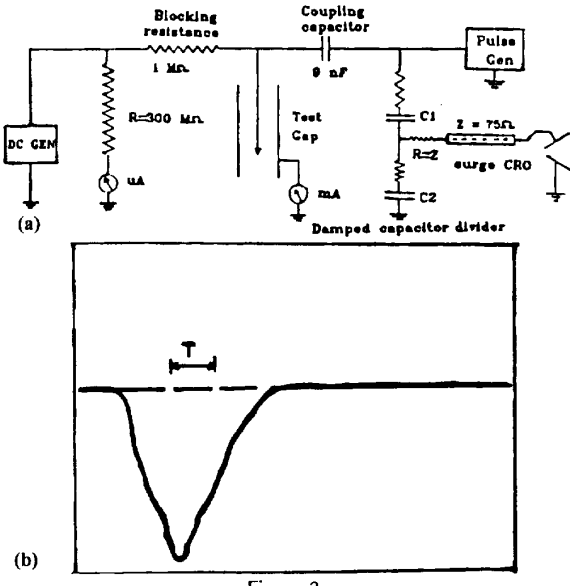

Figure 3.

dc + Pulse energization. (a) Circuit diagram, (b) typical pulse voltage of the RSG. T = 250 ns; pulse rise time = 250 ns, pulse width = 700 ns.

criteria were that each value of potential in the grid to be within 0.01% of its previous value and the current density at the plate be within 1% of the desired value.

3. EXPERIMENTAL STUDIES

To validate the predicted results experiments were carried out at negative pulse energization on a helical wire duct type ESP. The following wire configurations were used for study. 1 wire per section, 2 wires per section with wire-wire spacing of 9 cm and 15 cm, and 5 wires per section having 4.5 cm wire-wire spacing.

An additional parameter studied was the effect of dc bias. For each wire configuration the duct spacing was varied from 180 to 300 mm. The dc level, at each spacing, was varied from below corona onset to above corona onset point and VI characteristics were determined at each dc level. It should be noted that the current density in the pulse energization case refers to average collector current density.

Before obtaining the VI characteristics, studies were first conducted on the spark over characteristics of the duct type ESP under pulse energization, at three different pulse repetition rates *viz.* 50, 25 and 12.5 pulses per second. In this range, the effect of repetition rate on the sparkover characteristics is not so significant. But, a preliminary study of VI characteristics at these repetition rates, clearly show that the current density increases rapidly with increase in repetition rate. The study also

shows that at 50 pulses per second, the current density increases exponentially with increase in pulse voltage as compared to that at lower repetition rates. A further insight into these results are presented by the author in [20–22]. In the present work, the studies were carried out with a pulse repetition rate of 50, at which good electrical characteristics were obtained.

3.1. TEST GAP

Experiments were conducted on one section of a practical duct type ESP. The duct type geometry used in the present work corresponds to one section of a pilot plant precipitator. The wire-plate duct type ESP consists of two collector plates of 200 cm height and 50 cm width, with provision for suspending five helical wires in the center. The diameter and length of the corona wire were 2.7 mm and 183 cm, respectively. Each wire has a pitch of 9 cm, at which good corona characteristics were exhibited in a pipe type precipitator, as reported by Abdel-Salam *et al.* [23]. The wires were held under tension by two sets of copper rods mounted on two insulated supports. Provision was made to vary both the wire-wire and wire-plate spacings.

3.2. dc POWER SUPPLY

A dc power source of 250 kV, 25 mA rating (Kenotron Model) was used for the experimental studies. The set consists of a cascade connection of two voltage doublers each rating 125 kV. The output voltage could be varied from 10 to 250 kV. A precision 300 MΩ resistance was connected across the set, the current through which gives an indication of the output voltage. The minimum voltage that could be measured is 3 kV *i.e.* $\sim$ 1% of the total voltage. Provision has been made in the set to change the polarity of the output voltage.

3.3. REPETITIVE SURGE GENERATOR

The nanosecond voltage pulses were developed from a repetitive surge generator (GEC make). The generator is basically a MARX impulse circuit but with charging resistors replaced by inductances for quick charging of the capacitors. The generator consists of 7 stages of capacitors, each having a capacitance of 0.007 μF. The capacitors are charged in parallel by a 30 kV dc set. There is a centrally located insulated rod connected to the shaft of a motor mounted at the base of the pulse generator. Seven sets of brass electrodes are fixed to the insulating shaft which bridge a similar set of electrodes fixed to the capacitor terminals. The discharge of the capacitor is accomplished by the spark between the fixed and the rotating electrodes. Under normal operating conditions the generator produces 50 pulses per second. The pulse width is 700 ns with a rise time of 250 ns. A damped capacitance divider [Haefely, CZ-600] along with a Haefely peak voltmeter [type-65] and surge oscilloscope [Haefely, type-721], was used for voltage measurements.

For the pulse energization, a high resistance was used on the dc side to decouple the pulse, and a series capacitor was used on the pulse side to block dc. Figure 3(a) shows the schematic diagram of the circuit used for pulse energization and Figure 3(b) shows a typical pulse voltage waveform.

4. VALIDATION OF PULSE MODEL FOR DUCT TYPE ESP

A computer program has been written for the 1st and the 2nd part of the model. The numerical integrations, in the first part of the model, were carried out using Simpson's 1/3 method. The input parameters to the model are the duct spacing, wire-wire spacing, wire diameter and the dc voltage. For the 1st part of the model, the duct spacing was taken as the outer diameter of the cylinder (wire-cylinder model). For a given dc bias, the model begins with an initial estimation of pulse voltage. An average value of the dc +pulse voltage was found out and the calculations will proceed as explained in the previous Section.

Figures 4(a) to (f) show the validation of the proposed pulse model against the experimental results obtained during the present study. The dc bias in all cases is kept at or below corona onset. A close agreement with experimental results are obtained at lower pulse voltages and a maximum error of 10% results at higher pulse voltages. This is tolerable, given the various assumptions made in the model. The results are being presented for three types of wire configurations. For each type the predictions were made both at constant dc and at constant duct spacing.

It is worth mentioning that care should be taken in selecting the coefficients for attachment during the first part of modeling. In [15] it has been mentioned that η/p is negligible at $E/p > 0.45$ V/cm Pa . Assuming this concept results in overestimation of the results. But using Equation (19) gives fairly good results as it covers a wide range of η/p. The present pulse model has been tested only against the results of a laboratory scale ESP due to the lack of clean air experimental data of an industrial ESP operating under sub-microsecond pulse energization.

5. CONCLUSIONS

IT has been shown that there is a possibility of predicting pulse VI characteristics of a duct type ESP

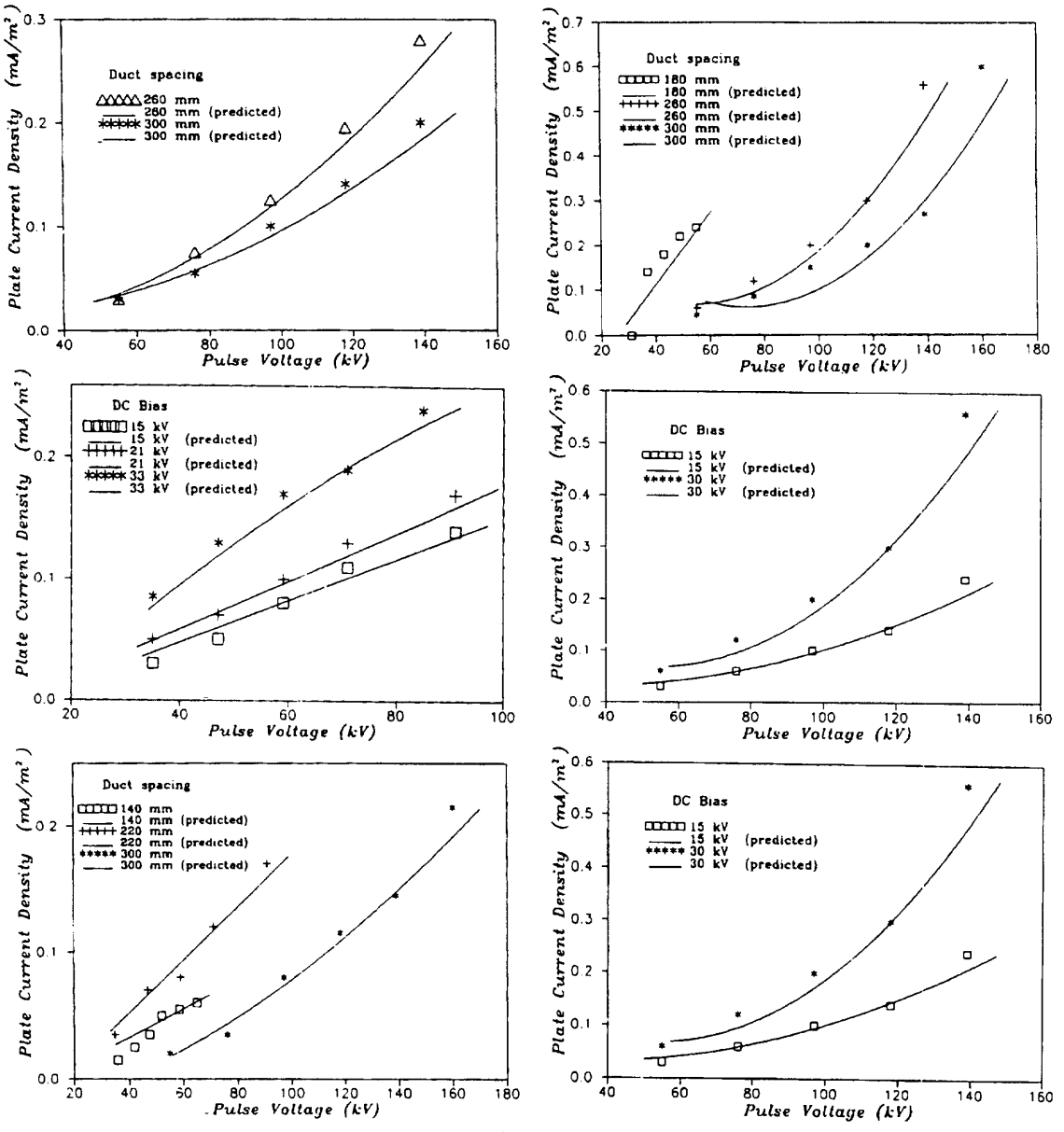

Figure 4.
Validation of theoretical predictions with experimental pulse VI data of duct type ESP.

based on Townsend theory and making use of an existing dc model. For modeling the corona processes near the wire a 1-dimensional model is adequate but it requires a 2-dimensional model for calculating the drift of the space charges. Given the precipitator geometry and the assumptions made, the proposed method is quite satisfactory in predicting the clean air VI characteristics.

REFERENCES

[1] S. Sekar and H. Stomberg, "On the Prediction of Current-voltage Characteristics for Wire-plate Precipitators", J. Electrostatics, No. 10, pp. 35–43, 1981.

[2] L. N. Menegozzi and P. L. Feldman, "The Physics of Pulse Energization in Electrostatic Precipitators", 3rd symp. Tranf. and Util. of particulate

control technology, Orlando, USA, 1981 (unpublished).

[3] L. Salasoo, J. K. Nelson, R. J. Schwabe and R. W. L. Snaddon, "Simulation and Measurement of Corona for Electrostatic Pulse Powered Precipitators", J. Appl. Phys., Vol. 58, No. 8, pp. 2949–2957, 1985.

[4] J. K. Nelson and L. Salasoo, "The Impact of Pulse Energization on Electrostatic Precipitator Performance", IEEE Trans. on EI, Vol. 22, No. 6, pp. 657–675, 1987.

[5] G. W. Penney and R. E. Mattick, "Potentials in dc Corona Fields", Trans. AIEE, Part I, Vol. 79, pp. 91–99, 1960.

[6] L. C. Thanh, "Negative Corona in Multiple Interacting Point to Plane Gap in Air", IEEE Trans. on IAS, Vol. 21, No. 2, pp. 518–522, 1985.

[7] E. Nasser, *Fundamentals of Gaseous Ionization and Plasma Electronics*, John Wiley & Sons. Inc., 1971.

[8] G. W. Trichel, "The Mechanism of Negative Point to Plane Corona near Onset", Phys. Rev., Vol. 54, No. 12, pp. 1078–1084, 1938.

[9] J. R. Mcdonald, W. B. Smith, H. W. Spencer Iii and L. E. Sparks, "A Mathematical Model for Calculating Electrical Conditions in Wire-duct Electrostatic Precipitator Devices", J. Appl. Phys., Vol. 48, No. 6, pp. 2231–2243, 1977.

[10] S. Oglesby, Jr. and G. B. Nichols, *Electrostatic Precipitation*, Marcel Dekker Inc., NY, USA, 1978.

[11] H. Raether, *Electron Avalanches and Breakdown in Gases*, Butterworth, Washington, 1964.k

[12] G. N. Aleksandrov, "On the Nature of Current Pulses of a Negative Corona", Sov. Phys. Tech. Phys., Vol. 8, N0. 2, pp. 161–166, 1963.

[13] R. Morrow, "Theory of Negative Corona in Oxygen", J. Appl. Phys., Vol. 32, No. 3, pp. 1799–1809, 1985.

[14] M. S. Abou-saeda and Kh. I. M. Ali, "Negative Corona Thresholds of Compressed SF_6 in Space Charge Modified Nonuniform Results", IEE conf. on Gas Disc. and Appl., No. 189, pp. 168–171, 1980.

[15] M. P. Sarma and W. Janischewskyj, "Dc Corona on Smooth Conductors in Air", Proc. IEE, Vol. 116, No. 1, pp. 161–166, 1969.

[16] M. Abdel-Salam and D. Wiitanen, "Calculation of Corona Onset Voltage for Duct Type Precipitators", IEEE IAS Annu. meet, Michigan, USA, pp. 720–724, 1991.

[17] M. Ogasawara, "Analysis of Formation Stage of Corona Discharge", J. Phys. Soc. Japan, Vol. 21, No. 11, pp. 2360–2372, 1966.

[18] V. E. Litvinov, "Method of Numerical Investigation of Volume Concentration of Charged Pigment Particles in the Process of Visualization of Electrostatic Images", J. of Electrostatics, Vol. 23, pp. 413–420, 1989.

[19] P. A. Lawless, "Modeling Particulate Charging in ESPs - Part II", IEEE IAS Annu. meet, California, USA, pp. 2154–2162, 1989.

[20] B. S. Rajanikanth and B. R. Prabhakar, "Sparkover Characteristics of Prototype Precipitator Subjected to dc/pulse Energization", Proc. IEEE IAS Annu. meet., Michigan, USA, pp. 729–733, 1991.

[21] B. S. Rajanikanth and B. R. Prabhakar, "Voltage-current Characteristics of Plate Type Precipitator Geometry under Combined dc/pulse Energizations", Proc. IEEE IAS Annu. meet., Michigan, USA, pp. 725–729, 1991.

[22] B. S. Rajanikanth, *Studies on the Voltage-current Characteristics of Duct Type Electrostatic Precipitators under dc/pulse Energizations*, Thesis, Indian Institute of Science, India, 1993.

[23] M. Abdel-Salam, M. El-Mohandes, A. A. Turkey and A. Yehia, "Analysis of Corona from Helical Wires", Proc. IEEE IAS Annu. meet., Pennsylvania, USA, pp. 1670–1676, 1988.

Manuscript was received on 20 September 1993, in final form 27 June 1994.